Scientific Reports

https://doi.org/10.1038/s41598-025-31615-9

Article in Press

Pulmonary toxicity of polymethyl methacrylate nanoplastics via intratracheal intubation in mice

Received: 27 August 2025

Accepted: 4 December 2025

Published online: 06 January 2026

Cite this article as: Youn C., Jo Y., Kwon J. *et al.* Pulmonary toxicity of polymethyl methacrylate nanoplastics via intratracheal intubation in mice. *Sci Rep* (2026). https://doi.org/10.1038/s41598-025-31615-9

Changsic Youn, Yu-Jin Jo, Jeongwoo Kwon, Seung-Bin Yoon, Hyeong-Ju You & Ji-Su Kim

Pulmonary Toxicity of Polymethyl methacrylate nanoplastics via Intratracheal Intubation in Mice

Changsic Youn[a,b#], Yu-Jin Jo[a#], Jeongwoo Kwon[a], Seung-Bin Yoon[a], Hyeong-Ju You[a], and Ji-Su Kim[a,b*]

[a]Primate Resources Center (PRC), Korea Research Institute of Bioscience and Biotechnology (KRIBB), Nengme-gil 351-33, Jeongeup-si, Jeollabuk-do, 56216, Republic of Korea

[b]UST Department of Functional Genomics, KRIBB School of Bioscience, Korea University of Science and Technology (UST), Daejeon, 34113, Republic of Korea

[#]These authors contributed equally to this work.

***Corresponding author**

Ji-Su Kim

Primate Resources Center (PRC), Korea Research Institute of Bioscience and Biotechnology (KRIBB), Nengme-gil 351-33, Jeongeup-si, Jeollabuk-do, 56216, Republic of Korea

Phone: +82-10-1234-5678

Fax: +82-063-570-5309

E-mail: kimjs@kribb.re.kr

Co-author e-mail addresses

Changsic Youn (zv40@kribb.re.kr)

Yu-Jin Jo (joyj@kribb.re.kr)

Jeongwoo Kwon (kwonjw@kribb.re.kr)

Seung-Bin Yoon (ellysbin@kribb.re.kr)

Hyeong-Ju You (hjyou@kribb.re.kr)

Abstract

Plastics, ubiquitous in daily life and industry, are released into the environment in substantial quantities. Instead of complete biodegradation, plastic waste fragments into smaller particles, accumulating as nanoplastics (NPs; <1 μm). Humans are exposed to NPs through inhalation and ingestion of contaminated water and food, which can induce cytotoxicity through physical and chemical pathways. Polymethyl methacrylate (PMMA), commonly used in implants and artificial bones, has been identified in human lungs and associated with pulmonary embolism. While PMMA NP toxicity has been reported in vitro, their in vivo effects, as well as the underlying mechanism, remain poorly understood. In this study, we investigated the pulmonary effects of inhaled PMMA NPs in mice. Mice received 20 or 100 μg of PMMA NPs (25 nm) via intratracheal intubation for 28 days. PMMA-NP preparation and characterization are described in the Methods section. Exposed mice exhibited body weight loss and pulmonary accumulation of PMMA NPs. Bronchoalveolar lavage fluid (BALF) analysis revealed increased cell count and elevated inflammatory cytokines in serum and BALF. Histopathology (H&E staining) revealed abnormalities in lung tissue and alterations in protein and RNA expression. The findings demonstrate that respiratory exposure to PMMA NPs induces lung inflammation, tissue damage, and molecular dysregulation.

Keywords: Nanoplastic, Lung toxicity, Intratracheal intubation, Inflammation, PMMA

Introduction

In modern society, plastics are extensively used, encompassing daily life, industry, medicine, and agriculture. Global plastic consumption is projected to increase

annually from 464 Mt in 2020 to 884 Mt by 2050 [1]. This increase will lead to a proportional rise in plastic waste, which is becoming a serious environmental concern. If current production and waste management trends persist, approximately 12,000 Mt of plastic waste will accumulate in landfills or leak into the environment by 2050, with severe consequences for the ecosystem [2]. Among plastic waste, microplastics (MPs; 1 μm to 1 mm) and nanoplastics (NPs; <1 μm), which are not visible to the naked eye, have emerged as contaminants of increasing ecological and public health concern. These MPs and NPs exist in various shapes (Spheres, fibers, and particles) and polymer types (e.g., polyethylene [PE], polystyrene [PS], polypropylene [PP], polyethylene terephthalate [PET], and polymethyl methacrylate [PMMA]) [3-5]. NPs generally accumulate in the environment through various degradation of larger plastics and MPs via mechanical abrasion, chemical oxidation, biodegradation, and photooxidation [6-13].

Due to their small size, NPs can easily cross cellular membranes, potentially exerting more severe impacts than MPs [14]. In marine environment, NPs can bioaccumulate and biomagnify in marine organisms ranging from phytoplankton, zooplankton, crustaceans, mollusks, and fish, resulting in impaired growth, altered development and reproduction, behavioral changes, and increased mortality [13,15-17]. This can disrupt the balance of marine ecosystems. NPs are also ubiquitous in the soil, where they can be ingested by soil microorganisms and animals, accumulate, disrupt plant physiology and induce oxidative stress, thereby affecting plant growth and biochemistry [18]. Humans can be exposed to MPs and NPs primarily through ingestion (contaminated food and water) and inhalation. Airborne particles can also penetrate the respiratory tract, reaching the lungs [19]. These plastic particles can accumulate in humans, and have been detected in human feces, lungs, brain, blood,

placenta, and saliva [20-25]. Their presence in various tissues and organs of the human body poses potential health risks. Multiple toxicological studies have been conducted on MP and NP. *In vitro* experiments showed that exposure to NPs causes various adverse effects, including disruption of intestinal epithelial tight junctions, oxidative stress, granulosa cell apoptosis, and hepatocyte fibrosis [26-30]. *In vivo* studies in mammals demonstrate that exposure can cause neurological dysfunction, liver and kidney damage, sperm quality deterioration, testicular and ovarian injury, and transplacental transfer of particles [26,28,29,31-34]. However, existing studies have limitations. First, *in vitro* experiments are limited because they cannot fully replicate the complex *in vivo* environment. Second, even during *in vivo* experiments, most studies simulate oral, dermal, or waterborne exposure, and only limited models directly exposed NPs through the respiratory system. Third, research tends to be biased toward certain types of plastics. For example, it has been shown that PMMA, which is widely used in medical procedures, such as vertebroplasty, has been implicated in postoperative pulmonary embolism and lung damage [35-37]. Although PMMA NPs are detected in the lungs of humans, *in vivo* studies on their pulmonary effects remain scarce. Therefore, investigating the pulmonary toxicity of PMMA-NPs is crucial, given their widespread medical use and their confirmed presence in human lungs. This study aims to address this gap by directly exposing animal models to NPs via the respiratory tract, thereby overcoming the limitations of previous studies. Recent studies have reported the presence of microplastics and nanoplastics, including PMMA fragments, in airborne samples collected indoors and outdoors [38,39]. This suggests that inhalation exposure is plausible under specific occupational or environmental conditions. In the present study, repeated intratracheal instillation was employed as a practical alternative to inhalation

exposure, enabling direct pulmonary deposition of nanoparticles with precise and reproducible dosing. The 28-day exposure period was chosen based on the framework of OECD Test Guideline 412 (Subacute Inhalation Studies). Intratracheal instillation was used as an exploratory model rather than a guideline-compliant regulatory study [40]. To assess the subacute effects of repeated exposure, we implemented a 28-day exposure regimen, consistent with standard toxicological assessment guidelines. Mice were exposed daily to PMMA NPs through intratracheal intubation and pulmonary toxicity was identified by monitoring diseases and symptoms that occurred in the tissues.

Results

NPs inhaled through the airways accumulate in the lungs

To investigate the effects of NP inhalation on the respiratory system, six-week-old mice were exposed to NPs daily via intratracheal intubation under respiratory anesthesia for 28 days (Fig. 1a). To confirm that the exposure to NPs via the respiratory system resulted in accumulation in the lungs, we performed *in vivo* fluorescence imaging (Fig. 1b). We observed that the fluorescence intensity significantly increased in the 100 μg group compared to the control group (Fig. 1c). To determine the effects on mice, we measured their body weight. Body weight gain was significantly reduced in the treatment group compared to that in the control group (Supplementary Data S1A and S1B), although no significant difference was observed in the lengths of the mice. However, the Lee index (length from the head to the anus relative to the body weight) and the body width of the mice were both significantly reduced in the treatment group (Supplementary Data S1B). These

results confirm that respiratory exposure to NPs leads to pulmonary accumulation and physiological changes.

Inhalation of NPs causes lung diseases

Bronchoalveolar lavage fluid (BALF) is typically used to determine the effect of NPs on the lungs and to evaluate lung injury [41,42]. We measured protein levels and changes in cell count in the BALF. Cell counts were significantly higher in the treatment group than that in the control group (Fig. 2a), and the bicinchoninic acid (BCA) assay also indicates a significant increase in total protein level in the treated groups (Fig. 2b). Next, H&E staining was performed to confirm lung disease. The invasion of immune and foam cells was confirmed in the treated group (Fig. 2c). Additionally, immunofluorescence imaging further confirmed NPs accumulation not only within lung tissue but also within inflammatory cells (Supplementary Data S2A). These results indicate that the respiratory exposure to NPs can result in lung disease.

Inhalation of NPs causes lung inflammation

NP exposure increased total cell counts, protein levels, and inflammatory cell infiltration in BALF. To confirm inflammation in the mice, serum levels of proinflammatory cytokines (IL-6, IL-1β, TNF-α) were measured. The results confirm that the levels of inflammatory cytokines were significantly increased in the 100 μg group (Fig. 3a). Next, we measured the levels of inflammatory cytokines in the BALF to confirm the occurrence of lung inflammation. The levels of IL-6, IL-1β, and TNF-α

were significantly increased in the 100 μg group and TNF-α was significantly increased in the 20 μg group (Fig. 3b). To confirm which inflammatory cell changes in the lungs caused the inflammation, we then measured the number of inflammatory cells (macrophages, lymphocytes, eosinophils, neutrophils, and basophils) using H&E staining in BALF. In the NP treatment group, the number of macrophages significantly decreased, whereas the numbers of lymphocytes and neutrophils significantly increased in the 100 μg group (Fig. 3c, 3d). Foamy macrophages were identified and their area ratio was significantly increased in the NPs treatment group (Fig. 3e). Additionally, immunofluorescence revealed that the intensity of foamy macrophages and lung damage CD36, as well as their colocalization with lung tissue, were significantly increased in the 100 μg group (Supplementary Data S2A, S2B and S2C)[43,44]. To determine whether the levels of inflammatory cytokines were elevated in the lung tissue, we examined both protein and mRNA levels. A significant increase in both protein and mRNA levels of inflammatory cytokines was observed in the 100 μg group (Fig. 3f, 3g, and 3h). These results confirm that respiratory exposure to NPs induces the formation of foamy macrophages and promotes lung inflammation.

Inhalation of NPs causes profibrotic activation

The results indicate abnormalities in the lung tissue. To investigate the potential induction of fibrotic responses, lung tissues exposed to NP were subjected to Sirius Red and Masson's trichrome staining (Fig. 4a and 4b). Quantitative analysis revealed that the percentage of Sirius Red–positive areas and Masson's trichrome–positive regions significantly increased in the NP-exposed group (Fig. 4c

and 4d). Histologically, NP-treated lungs exhibited peribronchial collagen accumulation and localized alveolar wall thickening (Fib. 4b); however, diffuse interstitial fibrosis was not observed. Correspondingly, protein expression levels of collagen type I (COL-1) and α-smooth muscle actin (α-SMA) markers associated with early profibrotic and myofibroblast activation were significantly elevated (Fig. 4e and 4f). These findings indicate that NP exposure initiates early profibrotic remodeling, rather than fully developed interstitial fibrosis, under the 28-day exposure conditions.

Discussion

The average adult airborne MP inhalation dose was approximately 5.18 x 10^{15} MPs/kg-BW/day [19], corresponding to far lower mass concentrations than used this study. We employed 20 μg and 100 μg as worst-case, mechanistic challenge doses to probe hazard pathways under extreme or cumulative exposure scenarios, consistent with prior intratracheal nanoplastic studies [45-47]. The dosing schedule followed the timeline of OECD Test Guideline (TG) 412 [40]. The 25 nm PMMA nanoparticles were selected because nanoparticles smaller than 100 nm are known to efficiently deposit in the alveolar region of the lung, facilitating deep pulmonary penetration and cellular internalization[48-50]. Clinical reports indicate that vertebroplasty can induce PMMA-associated pulmonary cement emboli. Even so the mechanism of vascular embolism differs from the airway exposure used in this study. Even so, reports of residual PMMA causing parenchymal lung pathology indicate that PMMA nanoparticle exposure may elicit similar adverse effects.

In this study, we investigated the effects of PMMA NPs on the respiratory system of mice. Our results reveal that mice exposed to PMMA NPs exhibit a significant

decrease in body weight gain, accompanied by reductions in the obesity index, Lee's index, and body width. Serum analysis further confirmed an increase in inflammatory cytokines, specifically IL-6, IL-1β, and TNF-α. These systemic inflammatory responses likely contribute to the reduced weight gain because IL-6 and TNF-α are known mediators of inflammatory-induced anorexia [51-54]. Additionally, increased energy expenditure due to lung injury and systemic inflammation may further contribute to weight loss. These results suggest that respiratory exposure to PMMA NPs can lead to local pulmonary toxicity, accompanied by systemic inflammatory responses and potential metabolic changes.

BALF analysis is widely used for evaluating lung disease in clinical settings. In this study, we observed a significant increase in both total cell counts and protein levels in the BALF. Elevated protein in the BALF can result from serum protein leakage across the air–blood barrier, local production by pulmonary immune and epithelial cells, including T cells, alveolar macrophages, bronchial epithelial cells, and alveolar epithelial cells type I and II [55]. Total cell counts in BALF commonly increases due to increase in immune cells during inflammation, profibrotic activation, smoking, and lung cancer [56-58]. Our results are consistent with these findings, showing a significant increase in BALF inflammatory cytokines, marked inflammatory cell infiltration in the lung tissue, and the formation of foamy macrophages, thus confirming the induction of lung inflammation.

Notably, the results of this study indicate the formation of foamy macrophages (foam cells, characterized by numerous cytoplasmic vacuoles) in the lung tissue and immune cells in the BALF. Foam cells arise when macrophages engulf excessive amounts of altered lipids (e.g., oxidized lipids) or particulates and accumulate them as lipid droplets in their cytoplasm. Beyond lipid storage, foam cells influence

immune responses by secreting inflammatory cytokines and altering antigen presentation [59]. Their presence has been consistently documented in various pulmonary pathological conditions, including inflammation, fibrosis, Chronic Obstructive Pulmonary Disease (COPD), tuberculosis, lung granuloma, and COVID-19 [60-64]. Previous research has shown that exposure to cigarette smoke, particulate matter, and nanosilica can induce lung diseases, such as inflammation, and cause macrophage dysfunction, leading to foam cell formation [65-68]. Consistent with this, our supplementary data confirm that PMMA NPs are primarily present in alveolar macrophages. This suggests that PMMA NPs may alter the lung environment through inflammation and promote differentiation into foam cells, potentially via lipid dysregulation within macrophages that internalize the NPs or direct cytotoxicity of the particles.

Immunofluorescence and further studies confirmed PMMA-NP uptake by macrophages and revealed a significant increase in the expression of the scavenging receptor CD36. Since CD36 is known to mediate the uptake of oxidized lipids and particulate matter, this suggests that macrophages can actively internalize PMMA NPs through a CD36-mediated pathway [69]. This mechanism is likely a critical first step in the cascade leading to foam cell formation, altered lipid metabolism, and inflammatory cytokine secretion. The increased CD36 expression suggests a potential molecular link between PMMA-NP exposure and the observed macrophage dysfunction and lung pathology. The cytokine elevations (IL-1β, IL-6, and TNF-α) observed are consistent with prior reports on polystyrene and polyethylene nanoplastics, indicating that pro-inflammatory activation is a common nanoplastic response [70-72]. CD36-mediated lipid uptake and foamy macrophage formation have similarly been described across various nanoparticle exposures [73-75],though

PMMA-NPs produced comparatively stronger CD36 induction in our study. In addition, increased COL-1 and α-SMA expression represents an early profibrotic signature broadly reported for nanoparticles[76-78]. These comparisons indicate that while many responses are shared across nanoplastics, PMMA-NPs may exhibit distinct effects on macrophage lipid metabolism. Further studies are needed to elucidate this direct interaction and its signaling pathways.

The results of the BALF analysis confirm that the proportions of neutrophils and lymphocytes increase following PMMA-NP exposure. This increase in the number of inflammatory cells in the lungs suggests that PMMA-NP exposure triggers an inflammatory response in the lungs. Neutrophils play an important role in innate immune responses to pathogens, such as bacteria and fungi, as well as to non-infectious stimuli. However, if inappropriately or excessively activated in the absence of infection, they secrete proteolytic enzymes and reactive oxygen species (ROS), leading to tissue injury and chronic inflammation [79-82]. Lymphocytes, comprising T cells, B cells, and natural killer (NK) cells, are vital components of the immune system. These specialized cells function in antibody production, direct cytotoxicity against virus-infected and tumor cells, and regulation of overall immune responses. When the immune system is activated, there's a noticeable increase in lymphocyte proliferation, which signals a robust and effective immune response [83]. Recruitment and activation of these immune cells in the lungs is regulated by proinflammatory cytokine. TNF-α and IL-1, activate vascular endothelial cells, facilitate cellular organization, and promote chemotaxis of macrophages and neutrophils to the lungs [84-88]. IL-6 is also a key player in immune responses and inflammation, and its expression and release are induced by various stimuli, including lipopolysaccharides (LPS), poly (I), poly (C), IL-1, tumor necrosis factor

(TNF), and platelet-derived growth factor [89-91]. In this inflammatory environment, alveolar macrophages can differentiate into foam cells by internalizing PMMA NPs. Foam cells are associated with chronic inflammation, and their formation may interfere with the immune function of macrophages [92]. Foamy macrophages can also secrete inflammatory cytokines (like IL-1 and IL-6), further promoting inflammation [59,93]. This suggests a cascade: PMMA-NP exposure damages and irritates the lung tissue, leading to an increased secretion of proinflammatory cytokines such as TNF-α and IL-1. This, in turn, recruits immune cells, such as neutrophils and lymphocytes, from the blood into the lungs. During this process, macrophages undergo lipid-induced differentiation into foam cells. It has been hypothesized that these foam cells further amplify the pulmonary inflammatory response by secreting inflammatory cytokines, such as IL-1 and IL-6, creating a self-perpetuating inflammatory cycle.

This study also confirmed an increased expression of collagen and α-SMA in lung tissue following PMMA-NP exposure, both of which are major indicators of fibrosis. This increase in proteins suggests that the lung tissue accumulates excessive extracellular matrix (ECM) in response to damage, activating fibroblasts and differentiating them into myofibroblasts [94,95]. Histological analysis revealed peribronchial collagen accumulation and alveolar wall thickening; however, diffuse interstitial fibrosis was not observed (Figure 4). While previous studies have shown that bleomycin-induced fibrosis begins to develop within 2–4 weeks, the establishment of persistent and mature interstitial fibrosis typically requires a longer duration (often ≥4–6 weeks) [96]. Therefore, the 28-day duration of this study was insufficient to induce mature fibrotic remodelling. Nevertheless, PMMA-NP induced alveolar wall thickening and increases in collagen I (COL1A1) and α-SMA markers of

early profibrotic/myofibroblast activation were observed at 28 days, suggesting initiation of profibrotic remodelling that may precede established lung fibrosis. Inflammatory cytokines of the IL-1 family (e.g., IL-1β, IL-18) are well-known major mediators of fibrosis [97]. In this study, both IL-1β and IL-18 in the PMMA NPs exposure group were significantly elevated compared to the control group, suggesting that exposure to PMMA NPs can induce an inflammatory response and promote pro fibotic activation. In addition, foam cells may also exacerbate fibrosis by secreting IL-1 family cytokines, stimulating surrounding cells, and reinforcing a fibrotic environment [59,98]. In this study, foamy macrophages were examined after exposure to PMMA NPs, suggesting that pro fibotic activation was induced by the secretion of fibrotic cytokines (IL-1 family) from damaged and inflamed tissues and foamy macrophages.

Although this study provides valuable insights into the pulmonary toxicity of PMMA NPs, it has several limitations. First, systemic effects were not evaluated. As shown in Supplementary Data S1, the weight loss observed after the exposure to PMMA NPs suggests possible systemic involvement. While such systemic effects have been predicted, impacting other organs as well, this study did not confirm them. Further studies are needed to confirm whether inhaled NPs translocate to other organs and induce pathological changes. Second, the conditions are limited. In atmospheric environments, MPs and NPs occur in various sizes, shapes, and chemical compositions exist in a complex manner [99,100]. However, only spherical PMMA NPs with a specific size (25 nm) were used in this study. Therefore, it is difficult to generalize the results of this study to human exposure scenarios and other types of plastics. Further comparative toxicological studies across a range of plastic

type and size are required. Third, a detailed mechanistic study is required. This study confirms that PMMA NPs cause lung inflammation and profibrotic activation; however, detailed mechanisms, such as the specific cellular and molecular signaling pathways that cause these pathological phenomena, have not been identified and in-depth research is required. Fourth, the focus of this study was placed on elucidating the toxicity of PMMA NPs. Approaches using rescue agents to alleviate or prevent their toxic effects (inflammation and profibrotic activation) were not explored. Follow-up rescue studies are required to reduce the health risks associated with NPs exposure. Fifth, this study was conducted using a single-sex cohort (female mice). Sex-specific differences can significantly influence the toxicological consequences of NP exposure. Therefore, while valuable, the results of this study may not be fully generalizable to all mice, regardless of gender. Future studies should include comparative studies between male and female mice to assess potential sex-specific differences in PMMA-NP toxicity and provide a more comprehensive risk assessment. Sixth, the intratracheal instillation method used here does not fully replicate chronic, low-dose inhalation exposure relevant to environmental conditions. Long-term aerosol inhalation studies are needed to evaluate real-world exposure patterns. Seventh, systemic biodistribution was not examined. Understanding whether PMMA NPs translocate beyond the lungs and accumulate in extrapulmonary organs is crucial for comprehensive hazard evaluation. Eighth, only a single PMMA NP type with fixed morphology and size was tested. Future studies should incorporate a wider variety of particle types, shapes, and physicochemical characteristics to better reflect environmental micro- and nanoplastic heterogeneity. Collectively, these limitations highlight the need for future studies that include both sexes, incorporate diverse particle types and sizes, assess

systemic biodistribution, and employ long-term aerosol inhalation models to more accurately represent real-world exposure and provide a comprehensive evaluation of PMMA-NP–related health risks. Addressing these limitations will provide insights into the potential health risks associated with NPs and facilitate the development of effective countermeasures.

In conclusion, this study evaluated the potential respiratory toxicity of PMMA NPs in humans through environmental inhalation exposure. Our findings confirm that inhaled PMMA NPs accumulate in the lung tissues, particularly within the cytoplasm of alveolar macrophages, and induce several pathological changes. Specifically, PMMA exposure triggers a pulmonary inflammatory response characterized by increased infiltration of inflammatory cells (e.g., neutrophils, lymphocytes) into the alveolar space and an increase in the secretion of inflammatory cytokines (e.g., IL-1β, IL-6, TNF-α). Furthermore, structural lung damage and pathological cellular changes, including profibrotic activation with excessive collagen deposition and foam cell formation, reflecting disrupted lipid metabolism and morphological alterations in macrophages. These findings suggest that PMMA NPs accumulate in the lungs and induce pulmonary inflammation, profibrotic activation, and changes in the distribution and differentiation of inflammatory cells, posing a significant threat to respiratory health.

Methods

Animals

All animal experiments were approved and conducted in accordance with the

guidelines of the Institutional Animal Care and Use Committee (IACUC) of Korea Research Institute of Bioscience and Biotechnology (KRIBB-AEC-24311). All animal procedures were performed in compliance with relevant institutional guidelines and regulations. This study's animal experiments are reported in accordance with the ARRIVE guidelines (http://arriveguidelines.org) to ensure transparency and reproducibility. Six- to seven-week-old female ICR mice were housed at 23 ± 1 °C under a 12-hour light/dark cycle, with food and water ad libitum.

Nanoparticle intratracheal intubation

PMMA NPs with a size of 25 nm (Cat No: 01-00-251), and the same particles conjugated with green fluorescent dye (Cat No: 29-00-251) were purchased from Micromod Partikeltechnologie GmbH (Rostock, Germany). Six-week-old mice weighing an average of 24–26 g were exposed to NPs via daily intratracheal intubation for 28 days. Mice were were anesthetized using 1.5% isoflurane inhalation in an induction chamber. Isoflurane was mixed with oxygen, and all anesthetic procedures were controlled using a anesthetic machine (ROYAL-77S; Elpis Medical, Gangwon-do, Korea) , and NPs were administered via a catheter. The control group received 50 μL of saline, and the treatment groups were exposed to 20 μg/50 μL and 100 μg/50 μL of NPs. Body weight was measured daily shortly before NP administration. Mice were sacrificed 24 h after the final exposure and samples were collected.

Preparation and analysis of bronchoalveolar lavage fluid

After 28 days of NP treatment, BALF was obtained by washing the lungs three times with 1 mL of saline. BALF was centrifuged at 300 × g for 7 min at 4 °C, and the supernatant was collected for Enzyme-Linked Immunosorbent Assay (ELISA) and BCA analysis. The pellet was resuspended in 200 μL of saline, and the saline was dried onto slides. Each slide was stained with hematoxylin and eosin (H&E), and 400 cells were selected. The slides were examined using a light microscope (ICC50 E, Leica Microsystems, Wetzlar, Germany). Individual cells were classified according to cell and nuclear morphology (basophils, characterized by the presence of numerous small granules; neutrophils, identified by 3–5 segmented nuclei; eosinophils, distinguished by pink-stained cytoplasm and bilobed nuclei; monocytes, identified by large nuclei; and macrophages, identified by irregular shape and smaller nuclei compared to monocytes).

Fluorescence measurements of the lungs

After 28 days of NP treatment, fluorescence imaging was performed using an *in vivo* imaging system (Uinv-420; Davinch-K, Seoul, Korea) to determine the accumulation of NPs in the lungs.

Histological analysis

Fixed lung tissues were processed for paraffin block production using an automated tissue processor (HistoCore PEARL; Leica Microsystems, Wetzlar, Germany) and paraffin embedding station (HistoCore Arcadia H; Leica Microsystems, Germany).

Paraffin blocks were sectioned at a thickness of 5 μm to produce slides, which were stained with H&E for histological analysis. Stained sections were visualized using a slide scanner (Aperio VERSA 8, Leica Microsystems, Germany) to determine the presence or absence of lung disease.

BALF and ELISA analysis

To measure protein levels in BALF, the supernatants were analyzed using the BCA Assay (Pierce™ BCA Protein Assay Kits, Thermo Fisher Scientific, Waltham, MA, USA). To assess systemic and pulmonary inflammatory cytokine levels (IL-6, IL-1β, TNF-α), serum and BALF samples were tested using ELISA kits (M6000B-1, MLB00C-1, MTA00B-1, R&D Systems, Minneapolis, USA) according to the manufacturer's instructions. BCA and ELISA signals were measured using a microplate reader (EPOCH2, BioTek, Vermont, USA).

Picosirius red staining

Paraffin-embedded lung tissue slides were deparaffinized three times with xylene for 15 min each, rehydrated twice with 100% ethanol for 1 min each and twice with 95% ethanol for 1 min each, and finally rehydrated in distilled water for 5 min. Lung tissue sections were stained with picrosirius red solution (ab150681; Abcam, Cambridge, UK) for 1 h and washed with 5% acetic acid. Finally, sections were dehydrated several times with ethanol, washed with xylene, and fixed with toluene. Lung tissue sections were stained with picrosirius red and visualized using a slide scanner (Aperio VERSA 8; Leica Microsystems, Germany).

Masson’s trichrome staining

deparaffinized lung tissue slides were stained using a trichrome staining kit (ab150686, Abcam, UK) according to the manufacturer's instructions. Lung tissue sections were stained with Masson's trichrome and visualized using a slide scanner (Aperio VERSA 8; Leica Microsystems, Germany).

Western blotting

Lung tissues were lysed using radioimmunoprecipitation assay (RIPA) lysis buffer (Pierce RIPA Buffer, 89901, Thermo Fisher Scientific, USA), and 1 mL PhosSTOP (PhosSTOP EASYpack; Roche, Chugai, Switzerland) was used for protein extraction. The tissue lysates were prepared using beads and incubated on ice for 10 min. The lysed tissues were centrifuged at 12,000 RPM for 30 min at 4 °C, and 500 µL of the supernatant was collected. Protein concentrations were measured using the BCA assay. Laemmli buffer containing beta-mercaptoethanol (#1610747, BIO RAD, California, USA) was added to the samples and boiled at 98 °C for 5 min. Proteins were separated using 10% SDS-PAGE (Sodium dodecyl sulfate polyacrylamide gel electrophoresis)(10% Mini-PROTEIN TGX Precast Protein Gels, BIO RAD) and transferred onto PVDF (Polyvinylidene difluoride) membranes. After blocking in Tris-buffered saline containing 0.25% Tween 20 (TBST) and 5% BSA for 1 h, the membranes were incubated with primary antibodies overnight at 4 °C. After washing with TBST, the membranes were incubated with horseradish peroxidase-conjugated secondary antibodies. Protein bands were visualized using

enhanced chemiluminescence (SuperSignal West Pico Plus; Thermo Fisher Scientific, USA) according to the manufacturer's instructions. Densitometric analysis for semi-quantification was performed using ImageJ software (version 1.47; NIH, Bethesda, MD, USA; http://imagej.nih.gov/ij).

Real-time quantitative polymerase chain reaction

Lung tissues were lysed with RIPA lysis buffer (89901; Pierce RIPA Buffer, Thermo Fisher Scientific, USA). Total RNA was then recovered from lung tissues using the RNeasy Mini Kit (74106, Qiagen, Venlo, Netherlands). Poly(A) mRNA was reverse-transcribed in a 20 μL reaction mixture containing oligo(dT)20 primer, 5X RT buffer, 10 U of RNase inhibitor ReverTra Ace (Toyobo, Osaka, Japan), and 10 mM dNTP (Deoxyribonucleoside triphosphate) mixture. Secondary RNA structures were denatured by reacting at 42 °C for 60 min to facilitate cDNA synthesis. The reaction was terminated by incubation at 99 °C for 5 min. The resulting cDNA was used as a template for polymerase chain reaction (PCR) amplification using the PowerUp SYBR Green Master Mix (Thermo Fisher Scientific, USA) on a StepOnePlus Real-Time PCR System (Thermo Fisher Scientific, USA). The PCR cycling conditions were 30 s at 95 °C, 30 s at 60 °C, and 30 s at 72 °C for 40 cycles, followed by an extended incubation at 72 °C for 5 min. The housekeeping gene H2A.Z RNA was used as the internal standard for each group. The mouse primers were designed using Primer3 (http://bioinfo.ebc.ee/mprimer3). The primer sequences are listed in Supplementary Table S1.

Statistical analysis

All data were first assessed for normality using the Shapiro-Wilk test. All datasets passed the normality assumption ($p > 0.05$) and were therefore not normalized or transformed. Differences between groups were evaluated using Ordinary One-way Analysis of Variance (ANOVA) followed by Dunnett's multiple comparison test. We confirm that all statistical analyses, as presented in the figures, relied on the Ordinary One-way ANOVA method. Sample sizes varied based on the specific assay requirements (n=3 for Western blotting, n=4 for RT-qPCR, n=5 for ELISA/Histology), a standard approach in *in vivo* studies to balance rigor and ethical animal use. Data are presented as the mean ± SEM.

Declaration of generative AI in scientific writing

This declaration does not apply to the use of AI for purposes beyond grammar and spell checking.

References

1 Dokl, M. *et al.* Global projections of plastic use, end-of-life fate and potential changes in consumption, reduction, recycling and replacement with bioplastics to 2050. *Sustainable Production and Consumption* **51**, 498-518, doi:https://doi.org/10.1016/j.spc.2024.09.025 (2024).

2 Geyer, R., Jambeck, J. R. & Law, K. L. Production, use, and fate of all plastics ever made. *Sci Adv* **3**, e1700782, doi:10.1126/sciadv.1700782 (2017).

3 Andoh, C. N., Attiogbe, F., Bonsu Ackerson, N. O., Antwi, M. & Adu-Boahen, K. Fourier Transform Infrared Spectroscopy: An analytical technique for microplastic identification and quantification. *Infrared Physics & Technology* **136**, 105070, doi:https://doi.org/10.1016/j.infrared.2023.105070 (2024).

4 Jakubowicz, I., Enebro, J. & Yarahmadi, N. Challenges in the search for nanoplastics in the environment—A critical review from the polymer science perspective. *Polymer Testing* **93**, 106953, doi:https://doi.org/10.1016/j.polymertesting.2020.106953 (2021).

5 Boughbina-Portolés, A. & Campíns-Falcó, P. Assessing the size transformation of nanoplastics in natural water matrices. *Science of The Total Environment* **953**, 176225, doi:https://doi.org/10.1016/j.scitotenv.2024.176225 (2024).

6 Wu, X. *et al.* Critical effect of biodegradation on long-term microplastic weathering in sediment environments: A systematic review. *Journal of Hazardous Materials* **437**, 129287, doi:https://doi.org/10.1016/j.jhazmat.2022.129287 (2022).

7 Chubarenko, I., Efimova, I., Bagaeva, M., Bagaev, A. & Isachenko, I. On mechanical fragmentation of single-use plastics in the sea swash zone with different types of bottom sediments: Insights from laboratory experiments. *Marine Pollution Bulletin* **150**, 110726, doi:https://doi.org/10.1016/j.marpolbul.2019.110726 (2020).

8 Li, M. *et al.* Cotransport and Deposition of Iron Oxides with Different-Sized Plastic Particles in Saturated Quartz Sand. *Environmental Science & Technology* **53**, 3547-3557, doi:10.1021/acs.est.8b06904 (2019).

9 Arp, H. P. H. *et al.* Weathering Plastics as a Planetary Boundary Threat: Exposure, Fate, and Hazards. *Environmental Science & Technology* **55**, 7246-7255, doi:10.1021/acs.est.1c01512 (2021).

10 Wu, X. *et al.* Photo aging and fragmentation of polypropylene food packaging materials in artificial seawater. *Water Research* **188**, 116456, doi:https://doi.org/10.1016/j.watres.2020.116456 (2021).

11 Wu, X. *et al.* Photo aging of polypropylene microplastics in estuary water and coastal seawater: Important role of chlorine ion. *Water Research* **202**, 117396, doi:https://doi.org/10.1016/j.watres.2021.117396 (2021).

12 Giacomucci, L., Raddadi, N., Soccio, M., Lotti, N. & Fava, F. Biodegradation of polyvinyl chloride plastic films by enriched anaerobic marine consortia. *Marine Environmental Research* **158**, 104949, doi:https://doi.org/10.1016/j.marenvres.2020.104949 (2020).

13 Barría, C., Brandts, I., Tort, L., Oliveira, M. & Teles, M. Effect of nanoplastics on fish health and performance: A review. *Marine Pollution Bulletin* **151**, 110791, doi:https://doi.org/10.1016/j.marpolbul.2019.110791 (2020).

14 Wang, W. *et al.* Effects of polyethylene microplastics on cell membranes: A combined study of experiments and molecular dynamics simulations. *J Hazard Mater* **429**, 128323, doi:10.1016/j.jhazmat.2022.128323 (2022).

15 Zaki, M. R. M. & Aris, A. Z. An overview of the effects of nanoplastics on marine organisms. *Science of The Total Environment* **831**, 154757, doi:https://doi.org/10.1016/j.scitotenv.2022.154757 (2022).

16 Ferreira, I., Venâncio, C., Lopes, I. & Oliveira, M. Nanoplastics and marine organisms: What has been studied? *Environmental Toxicology and Pharmacology* **67**, 1-7,

doi:https://doi.org/10.1016/j.etap.2019.01.006 (2019).

17 Gonçalves, J. M. & Bebianno, M. J. Nanoplastics impact on marine biota: A review. *Environmental Pollution* **273**, 116426, doi:https://doi.org/10.1016/j.envpol.2021.116426 (2021).

18 Pérez-Reverón, R. *et al.* Nanoplastics in the soil environment: Analytical methods, occurrence, fate and ecological implications. *Environmental Pollution* **317**, 120788, doi:https://doi.org/10.1016/j.envpol.2022.120788 (2023).

19 Eberhard, T., Casillas, G., Zarus, G. M. & Barr, D. B. Systematic review of microplastics and nanoplastics in indoor and outdoor air: identifying a framework and data needs for quantifying human inhalation exposures. *J Expo Sci Environ Epidemiol* **34**, 185-196, doi:10.1038/s41370-023-00634-x (2024).

20 Yan, Z. *et al.* Analysis of Microplastics in Human Feces Reveals a Correlation between Fecal Microplastics and Inflammatory Bowel Disease Status. *Environmental Science & Technology* **56**, 414-421, doi:10.1021/acs.est.1c03924 (2022).

21 Amato-Lourenço, L. F. *et al.* Presence of airborne microplastics in human lung tissue. *Journal of Hazardous Materials* **416**, 126124, doi:https://doi.org/10.1016/j.jhazmat.2021.126124 (2021).

22 Abbasi, S. & Turner, A. Human exposure to microplastics: A study in Iran. *Journal of Hazardous Materials* **403**, 123799, doi:https://doi.org/10.1016/j.jhazmat.2020.123799 (2021).

23 Nihart, A. J. *et al.* Bioaccumulation of microplastics in decedent human brains. *Nature Medicine*, doi:10.1038/s41591-024-03453-1 (2025).

24 Leslie, H. A. *et al.* Discovery and quantification of plastic particle pollution in human blood. *Environment International* **163**, 107199, doi:https://doi.org/10.1016/j.envint.2022.107199 (2022).

25 Ragusa, A. *et al.* Plasticenta: First evidence of microplastics in human placenta. *Environment International* **146**, 106274, doi:https://doi.org/10.1016/j.envint.2020.106274 (2021).

26 Xu, D., Ma, Y., Han, X. & Chen, Y. Systematic toxicity evaluation of polystyrene nanoplastics on mice and molecular mechanism investigation about their internalization into Caco-2 cells. *Journal of Hazardous Materials* **417**, 126092, doi:https://doi.org/10.1016/j.jhazmat.2021.126092 (2021).

27 Domenech, J. *et al.* Long-Term Effects of Polystyrene Nanoplastics in Human Intestinal Caco-2 Cells. *Biomolecules* **11** (2021).

28 An, R. *et al.* Polystyrene microplastics cause granulosa cells apoptosis and fibrosis in ovary through oxidative stress in rats. *Toxicology* **449**, 152665, doi:https://doi.org/10.1016/j.tox.2020.152665 (2021).

29 Shen, R. *et al.* Accumulation of polystyrene microplastics induces liver fibrosis by activating cGAS/STING pathway. *Environmental Pollution* **300**, 118986, doi:https://doi.org/10.1016/j.envpol.2022.118986 (2022).

30 Chen, Y.-C. *et al.* The nephrotoxic potential of polystyrene microplastics at realistic

environmental concentrations. *Journal of Hazardous Materials* **427**, 127871, doi:https://doi.org/10.1016/j.jhazmat.2021.127871 (2022).

31 Yang, Q. *et al.* Oral feeding of nanoplastics affects brain function of mice by inducing macrophage IL-1 signal in the intestine. *Cell Reports* **42**, 112346, doi:https://doi.org/10.1016/j.celrep.2023.112346 (2023).

32 Wang, X. *et al.* Effects of polystyrene nanoplastic gestational exposure on mice. *Chemosphere* **324**, 138255, doi:https://doi.org/10.1016/j.chemosphere.2023.138255 (2023).

33 Jin, H. *et al.* Polystyrene microplastics induced male reproductive toxicity in mice. *Journal of Hazardous Materials* **401**, 123430, doi:https://doi.org/10.1016/j.jhazmat.2020.123430 (2021).

34 Fournier, S. B. *et al.* Nanopolystyrene translocation and fetal deposition after acute lung exposure during late-stage pregnancy. *Particle and Fibre Toxicology* **17**, 55, doi:10.1186/s12989-020-00385-9 (2020).

35 Myers, S. D., Jr., Streiff, M., Dulberger, A. R., American, M. & Sanders, C. D. Polymethylmethacrylate Pulmonary Embolism Following Vertebroplasty. *Cureus* **13**, e17314, doi:10.7759/cureus.17314 (2021).

36 Rodriguez-Arguisjuela, M. *et al.* Lung injury in patients age 75 years and older with the use of polymethylmethacrylate fenestrated pedicle screws. *Spine J* **21**, 430-437, doi:10.1016/j.spinee.2020.11.006 (2021).

37 Venmans, A., Lohle, P. N. M., van Rooij, W. J., Verhaar, H. J. J. & Mali, W. P. T. M. Frequency and Outcome of Pulmonary Polymethylmethacrylate Embolism during Percutaneous Vertebroplasty. *American Journal of Neuroradiology* **29**, 1983, doi:10.3174/ajnr.A1269 (2008).

38 Bhat, M. A. Airborne microplastic contamination across diverse university indoor environments: A comprehensive ambient analysis. *Air Quality, Atmosphere & Health* **17**, 1851-1866, doi:10.1007/s11869-024-01548-9 (2024).

39 Gossmann, I. *et al.* Occurrence and backtracking of microplastic mass loads including tire wear particles in northern Atlantic air. *Nat Commun* **14**, 3707, doi:10.1038/s41467-023-39340-5 (2023).

40 Development(OECD), O. f. E. C.-o. a. Test No. 412: Subacute Inhalation Toxicity: 28-Day Study. (2018).

41 Zielonka, T. M., Wałajtys-Rode, E., Chazan, R. & Droszcz, W. [Extracellular components of bronchoalveolar lavage fluid (BALF) as a marker of interstitial pulmonary disease activity. I. Protein concentration]. *Przegl Lek* **55**, 581-585 (1998).

42 Davidson, K. R., Ha, D. M., Schwarz, M. I. & Chan, E. D. Bronchoalveolar lavage as a diagnostic procedure: a review of known cellular and molecular findings in various lung diseases. *J Thorac Dis* **12**, 4991-5019, doi:10.21037/jtd-20-651 (2020).

43 Hayden, J. M. *et al.* Induction of monocyte differentiation and foam cell formation in vitro by 7-ketocholesterol. *J Lipid Res* **43**, 26-35 (2002).

44 Kwak, D. *et al.* CD36/Lyn kinase interactions within macrophages promotes pulmonary fibrosis in response to oxidized phospholipid. *Respir Res* **24**, 314,

doi:10.1186/s12931-023-02629-6 (2023).

45 Yang, S. *et al.* Inhalation exposure to polystyrene nanoplastics induces chronic obstructive pulmonary disease-like lung injury in mice through multi-dimensional assessment. *Environ Pollut* **347**, 123633, doi:10.1016/j.envpol.2024.123633 (2024).

46 Zhang, T. *et al.* Multi-dimensional evaluation of cardiotoxicity in mice following respiratory exposure to polystyrene nanoplastics. *Part Fibre Toxicol* **20**, 46, doi:10.1186/s12989-023-00557-3 (2023).

47 Wang, Q. *et al.* Polystyrene nanoplastics aggravate house dust mite induced allergic airway inflammation through EGFR/ERK-dependent lung epithelial barrier dysfunction. *Ecotoxicol Environ Saf* **298**, 118329, doi:10.1016/j.ecoenv.2025.118329 (2025).

48 Geiser, M. & Kreyling, W. G. Deposition and biokinetics of inhaled nanoparticles. *Part Fibre Toxicol* **7**, 2, doi:10.1186/1743-8977-7-2 (2010).

49 Sukhanova, A. *et al.* Dependence of Nanoparticle Toxicity on Their Physical and Chemical Properties. *Nanoscale Res Lett* **13**, 44, doi:10.1186/s11671-018-2457-x (2018).

50 Gonzalez-Vega, J. G. *et al.* Lung Models to Evaluate Silver Nanoparticles' Toxicity and Their Impact on Human Health. *Nanomaterials (Basel)* **12**, doi:10.3390/nano12132316 (2022).

51 Hunschede, S., Kubant, R., Akilen, R., Thomas, S. & Anderson, G. H. Decreased Appetite after High-Intensity Exercise Correlates with Increased Plasma Interleukin-6 in Normal-Weight and Overweight/Obese Boys. *Curr Dev Nutr* **1**, e000398, doi:10.3945/cdn.116.000398 (2017).

52 Patsalos, O., Dalton, B. & Himmerich, H. Effects of IL-6 Signaling Pathway Inhibition on Weight and BMI: A Systematic Review and Meta-Analysis. *International Journal of Molecular Sciences* **21** (2020).

53 Romanatto, T. *et al.* TNF-alpha acts in the hypothalamus inhibiting food intake and increasing the respiratory quotient--effects on leptin and insulin signaling pathways. *Peptides* **28**, 1050-1058, doi:10.1016/j.peptides.2007.03.006 (2007).

54 Patsalos, O., Dalton, B., Leppanen, J., Ibrahim, M. A. A. & Himmerich, H. Impact of TNF-α Inhibitors on Body Weight and BMI: A Systematic Review and Meta-Analysis. *Front Pharmacol* **11**, 481, doi:10.3389/fphar.2020.00481 (2020).

55 Noël-Georis, I., Bernard, A., Falmagne, P. & Wattiez, R. Database of bronchoalveolar lavage fluid proteins. *Journal of Chromatography B* **771**, 221-236, doi:https://doi.org/10.1016/S1570-0232(02)00114-9 (2002).

56 Domagała-Kulawik, J., Skirecki, T., Maskey-Warzechowska, M., Grubek-Jaworska, H. & Chazan, R. Bronchoalveolar lavage total cell count in interstitial lung diseases--does it matter? *Inflammation* **35**, 803-809, doi:10.1007/s10753-011-9378-5 (2012).

57 Yang, Y. *et al.* Bronchoalveolar Lavage Fluid-Derived Exosomes: A Novel Role Contributing to Lung Cancer Growth. *Front Oncol* **9**, 197, doi:10.3389/fonc.2019.00197 (2019).

58 Sobiecka, M. *et al.* Bronchoalveolar Lavage Cell Count and Lymphocytosis Are the Important Discriminators between Fibrotic Hypersensitivity Pneumonitis and Idiopathic Pulmonary Fibrosis. *Diagnostics (Basel)* **13**, doi:10.3390/diagnostics13050935 (2023).

59 Agarwal, P., Gordon, S. & Martinez, F. O. Foam Cell Macrophages in Tuberculosis. *Front Immunol* **12**, 775326, doi:10.3389/fimmu.2021.775326 (2021).

60 Romero, F. *et al.* A pneumocyte-macrophage paracrine lipid axis drives the lung toward fibrosis. *Am J Respir Cell Mol Biol* **53**, 74-86, doi:10.1165/rcmb.2014-0343OC (2015).

61 Hsieh, M. H. *et al.* Surfactant protein D inhibits lipid-laden foamy macrophages and lung inflammation in chronic obstructive pulmonary disease. *Cell Mol Immunol* **20**, 38-50, doi:10.1038/s41423-022-00946-2 (2023).

62 Ordway, D., Henao-Tamayo, M., Orme, I. M. & Gonzalez-Juarrero, M. Foamy macrophages within lung granulomas of mice infected with Mycobacterium tuberculosis express molecules characteristic of dendritic cells and antiapoptotic markers of the TNF receptor-associated factor family. *J Immunol* **175**, 3873-3881, doi:10.4049/jimmunol.175.6.3873 (2005).

63 Chrabańska, M., Mazur, A. & Stęplewska, K. Histopathological pulmonary findings of survivors and autopsy COVID-19 cases: A bi-center study. *Medicine* **101** (2022).

64 Zhu, Y., Choi, D., Somanath, P. R. & Zhang, D. Lipid-Laden Macrophages in Pulmonary Diseases. *Cells* **13**, doi:10.3390/cells13110889 (2024).

65 Pramanik, S. & Sil, A. K. Cigarette smoke extract induces foam cell formation by impairing machinery involved in lipid droplet degradation. *Pflugers Arch* **476**, 59-74, doi:10.1007/s00424-023-02870-4 (2024).

66 Liu, J. *et al.* PM2.5 aggravates the lipid accumulation, mitochondrial damage and apoptosis in macrophage foam cells. *Environmental Pollution* **249**, 482-490, doi:https://doi.org/10.1016/j.envpol.2019.03.045 (2019).

67 Cao, Y. *et al.* Foam cell formation by particulate matter (PM) exposure: a review. *Inhal Toxicol* **28**, 583-590, doi:10.1080/08958378.2016.1236157 (2016).

68 Guo, C. *et al.* Silica nanoparticles promoted pro-inflammatory macrophage and foam cell transformation via ROS/PPARγ/NF-κB signaling. *Science of The Total Environment* **881**, 163430, doi:https://doi.org/10.1016/j.scitotenv.2023.163430 (2023).

69 Xu, S. *et al.* Uptake of oxidized lipids by the scavenger receptor CD36 promotes lipid peroxidation and dysfunction in CD8(+) T cells in tumors. *Immunity* **54**, 1561-1577 e1567, doi:10.1016/j.immuni.2021.05.003 (2021).

70 Li, X. *et al.* Intratracheal administration of polystyrene microplastics induces pulmonary fibrosis by activating oxidative stress and Wnt/beta-catenin signaling pathway in mice. *Ecotoxicol Environ Saf* **232**, 113238, doi:10.1016/j.ecoenv.2022.113238 (2022).

71 Kwabena Danso, I., Woo, J. H., Hoon Baek, S., Kim, K. & Lee, K. Pulmonary toxicity assessment of polypropylene, polystyrene, and polyethylene microplastic fragments in mice. *Toxicol Res* **40**, 313-323, doi:10.1007/s43188-023-00224-x (2024).

72 Gou, Z., Wu, H., Li, S., Liu, Z. & Zhang, Y. Airborne micro- and nanoplastics: emerging causes of respiratory diseases. *Part Fibre Toxicol* **21**, 50, doi:10.1186/s12989-024-00613-6 (2024).

73 Woo, J. H. *et al.* Polypropylene nanoplastic exposure leads to lung inflammation through

p38-mediated NF-kappaB pathway due to mitochondrial damage. *Part Fibre Toxicol* **20**, 2, doi:10.1186/s12989-022-00512-8 (2023).

74 Jin, Y. J. *et al.* Characterisation of changes in global genes expression in the lung of ICR mice in response to the inflammation and fibrosis induced by polystyrene nanoplastics inhalation. *Toxicol Res* **39**, 1-25, doi:10.1007/s43188-023-00188-y (2023).

75 Ma, R. *et al.* Amorphous silica nanoparticles accelerated atherosclerotic lesion progression in ApoE(-/-) mice through endoplasmic reticulum stress-mediated CD36 up-regulation in macrophage. *Part Fibre Toxicol* **17**, 50, doi:10.1186/s12989-020-00380-0 (2020).

76 Gibb, A. A., Lazaropoulos, M. P. & Elrod, J. W. Myofibroblasts and Fibrosis: Mitochondrial and Metabolic Control of Cellular Differentiation. *Circ Res* **127**, 427-447, doi:10.1161/CIRCRESAHA.120.316958 (2020).

77 Zhang, Y. *et al.* Coal dust nanoparticles induced pulmonary fibrosis by promoting inflammation and epithelial-mesenchymal transition via the NF-kappaB/NLRP3 pathway driven by IGF1/ROS-mediated AKT/GSK3beta signals. *Cell Death Discov* **8**, 500, doi:10.1038/s41420-022-01291-z (2022).

78 Zhang, G. *et al.* Titanium nanoparticles released from orthopedic implants induce muscle fibrosis via activation of SNAI2. *J Nanobiotechnology* **22**, 522, doi:10.1186/s12951-024-02762-4 (2024).

79 Giacalone, V. D., Margaroli, C., Mall, M. A. & Tirouvanziam, R. Neutrophil Adaptations upon Recruitment to the Lung: New Concepts and Implications for Homeostasis and Disease. *Int J Mol Sci* **21**, doi:10.3390/ijms21030851 (2020).

80 Kessenbrock, K., Dau, T. & Jenne, D. E. Tailor-made inflammation: how neutrophil serine proteases modulate the inflammatory response. *J Mol Med (Berl)* **89**, 23-28, doi:10.1007/s00109-010-0677-3 (2011).

81 Veenith, T. *et al.* High generation of reactive oxygen species from neutrophils in patients with severe COVID-19. *Scientific Reports* **12**, 10484, doi:10.1038/s41598-022-13825-7 (2022).

82 Nguyen, G. T., Green, E. R. & Mecsas, J. Neutrophils to the ROScue: Mechanisms of NADPH Oxidase Activation and Bacterial Resistance. *Front Cell Infect Microbiol* **7**, 373, doi:10.3389/fcimb.2017.00373 (2017).

83 Larosa, D. F. & Orange, J. S. 1. Lymphocytes. *J Allergy Clin Immunol* **121**, S364-369; quiz S412, doi:10.1016/j.jaci.2007.06.016 (2008).

84 Ott, L. W. *et al.* Tumor Necrosis Factor-alpha- and interleukin-1-induced cellular responses: coupling proteomic and genomic information. *J Proteome Res* **6**, 2176-2185, doi:10.1021/pr060665l (2007).

85 Dinarello, C. A. Proinflammatory Cytokines. *Chest* **118**, 503-508, doi:https://doi.org/10.1378/chest.118.2.503 (2000).

86 Kwon, H.-J. *et al.* Tumor Necrosis Factor Alpha Induction of NF-κB Requires the Novel Coactivator SIMPL. *Molecular and Cellular Biology* **24**, 9317-9326, doi:10.1128/MCB.24.21.9317-9326.2004 (2004).

87 Vig, E. *et al.* SIMPL Is a Tumor Necrosis Factor-specific Regulator of Nuclear Factor-κB Activity *. *Journal of Biological Chemistry* **276**, 7859-7866, doi:10.1074/jbc.M010399200 (2001).

88 Vig, E. *et al.* Modulation of Tumor Necrosis Factor and Interleukin-1-dependent NF-κB Activity by mPLK/IRAK *. *Journal of Biological Chemistry* **274**, 13077-13084, doi:10.1074/jbc.274.19.13077 (1999).

89 Tosato, G. & Jones, K. D. Interleukin-1 induces interleukin-6 production in peripheral blood monocytes. *Blood* **75**, 1305-1310 (1990).

90 Confalone, E., D'Alessio, G. & Furia, A. IL-6 Induction by TNFα and IL-1β in an Osteoblast-Like Cell Line. *Int J Biomed Sci* **6**, 135-140 (2010).

91 Wang, Z. Y. & Bjorling, D. E. Tumor necrosis factor-α induces expression and release of interleukin-6 by human urothelial cells. *Inflamm Res* **60**, 525-532, doi:10.1007/s00011-010-0298-x (2011).

92 Angelovich, T. A., Hearps, A. C. & Jaworowski, A. Inflammation-induced foam cell formation in chronic inflammatory disease. *Immunol Cell Biol* **93**, 683-693, doi:10.1038/icb.2015.26 (2015).

93 Guerrini, V. & Gennaro, M. L. Foam Cells: One Size Doesn't Fit All. *Trends Immunol* **40**, 1163-1179, doi:10.1016/j.it.2019.10.002 (2019).

94 Zhang, H. Y., Gharaee-Kermani, M., Zhang, K., Karmiol, S. & Phan, S. H. Lung fibroblast alpha-smooth muscle actin expression and contractile phenotype in bleomycin-induced pulmonary fibrosis. *Am J Pathol* **148**, 527-537 (1996).

95 Mei, Q., Liu, Z., Zuo, H., Yang, Z. & Qu, J. Idiopathic Pulmonary Fibrosis: An Update on Pathogenesis. *Front Pharmacol* **12**, 797292, doi:10.3389/fphar.2021.797292 (2021).

96 Degryse, A. L. & Lawson, W. E. Progress toward improving animal models for idiopathic pulmonary fibrosis. *Am J Med Sci* **341**, 444-449, doi:10.1097/MAJ.0b013e31821aa000 (2011).

97 Borthwick, L. A. The IL-1 cytokine family and its role in inflammation and fibrosis in the lung. *Semin Immunopathol* **38**, 517-534, doi:10.1007/s00281-016-0559-z (2016).

98 Newby, A. & Thomas, A. Foam cell formation in vivo is pro-fibrotic. *Atherosclerosis* **241**, e81-e82, doi:10.1016/j.atherosclerosis.2015.04.286 (2015).

99 Choudhury, A. *et al.* Atmospheric microplastic and nanoplastic: The toxicological paradigm on the cellular system. *Ecotoxicology and Environmental Safety* **259**, 115018, doi:https://doi.org/10.1016/j.ecoenv.2023.115018 (2023).

100 Luo, D. *et al.* Micro- and nano-plastics in the atmosphere: A review of occurrence, properties and human health risks. *Journal of Hazardous Materials* **465**, 133412, doi:https://doi.org/10.1016/j.jhazmat.2023.133412 (2024).

Acknowledgements

This work was supported by the Korea Research Institute of Bioscience and Biotechnology (KRIBB) Research Initiative Program [grant number KGM5162524].

Author contributions

Changsic Youn: Writing – original draft, Methodology, Investigation, Formal analysis, and Data curation.

Yu-Jin Jo: Writing – original draft, Methodology, Investigation, Formal analysis, Data curation, and Conceptualization.

Jeongwoo Kwon: Writing – review and editing, Resources, Data curation.

Seung-Bin Yoon: Writing – review and editing, Resources, Data curation.

Hyeong-Ju You: Resources, Data curation.

Ji-Su Kim: Writing – review and editing, Visualization, Supervision, Project administration, Funding acquisition, and Conceptualization.

Data availability

The data supporting the findings of this study are available from the corresponding author upon request.

Funding declaration

This research was supported by the Korea Research Institute of Bioscience and Biotechnology (KRIBB) Research Initiative Program (KGM5162524).

Competing interests

The authors declare that they have no competing financial interests or personal relationships that may have influenced the work reported in this study.

Figure captions

Figure 1. Nanoplastics (NPs) inhaled through the airways accumulate in the lungs. (A) Schematic representation of the animal study design assessing the effects of NPs. (B, C) Green fluorescence of the whole lung tissue photographed with the in vivo imaging system. The fluorescence intensity was measured (n = 5, ordinary one-way ANOVA). Data are presented as the mean ± SEM. ***p < 0.001.

Figure 2. Inhalation of NPs causes lung disease. (A, B) Cell counts and protein concentrations were quantified in bronchoalveolar lavage fluid (BALF; n = 5, ordinary

one-way ANOVA). (C) Lung tissues were stained with hematoxylin and eosin (H&E). Blue arrows indicate macrophage, black arrows indicate foamy macrophages, and red arrows indicate lymphocytic infiltration. Data are presented as the mean ± SEM. *p < 0.05, ***p < 0.001.

Figure 3. NPs inhaled through the airways induce lung inflammation. (A, B) The levels of inflammatory cytokines in serum and bronchoalveolar lavage fluid (BALF) were measured using ELISA (n = 5, ordinary one-way ANOVA). (C, D) BALF cells were stained with hematoxylin and eosin staining (H&E) and 400 immune cells per mouse were classified (n = 5, ordinary one-way ANOVA). Black, red, blue, orange, and green squares represent alveolar macrophages, foamy macrophages, lymphocytes, represent eosinophils, and neutrophils, respectively. The area of 100 macrophages per mouse was measured (n = 5, ordinary one-way ANOVA). Inflammatory cytokine protein levels in lung tissue were determined by Western blotting (n = 3, ordinary one-way ANOVA). Inflammatory cytokine mRNA levels in lung tissue were determined by RT-qPCR (n = 4, ordinary one-way ANOVA). Data are presented as the mean ± SEM. **p < 0.01, ***p < 0.001.

Figure 4. NPs inhaled through the airways induce lung profibrotic activation. (A,B) Lung tissue slides were stained with Sirius red and Masson's trichrome to confirm fibrosis. (C, D) The percentage of fibrotic tissue is represented in a chart (n = 5, ordinary one-way ANOVA). (E) Fibrosis-related proteins were analyzed by Western blotting (n = 3, ordinary one-way ANOVA). Data are presented as the mean ± SEM.

*p < 0.05, **p < 0.01, ***p < 0.001.

Result 1. NPs inhaled through the airways accumulate in the lungs.

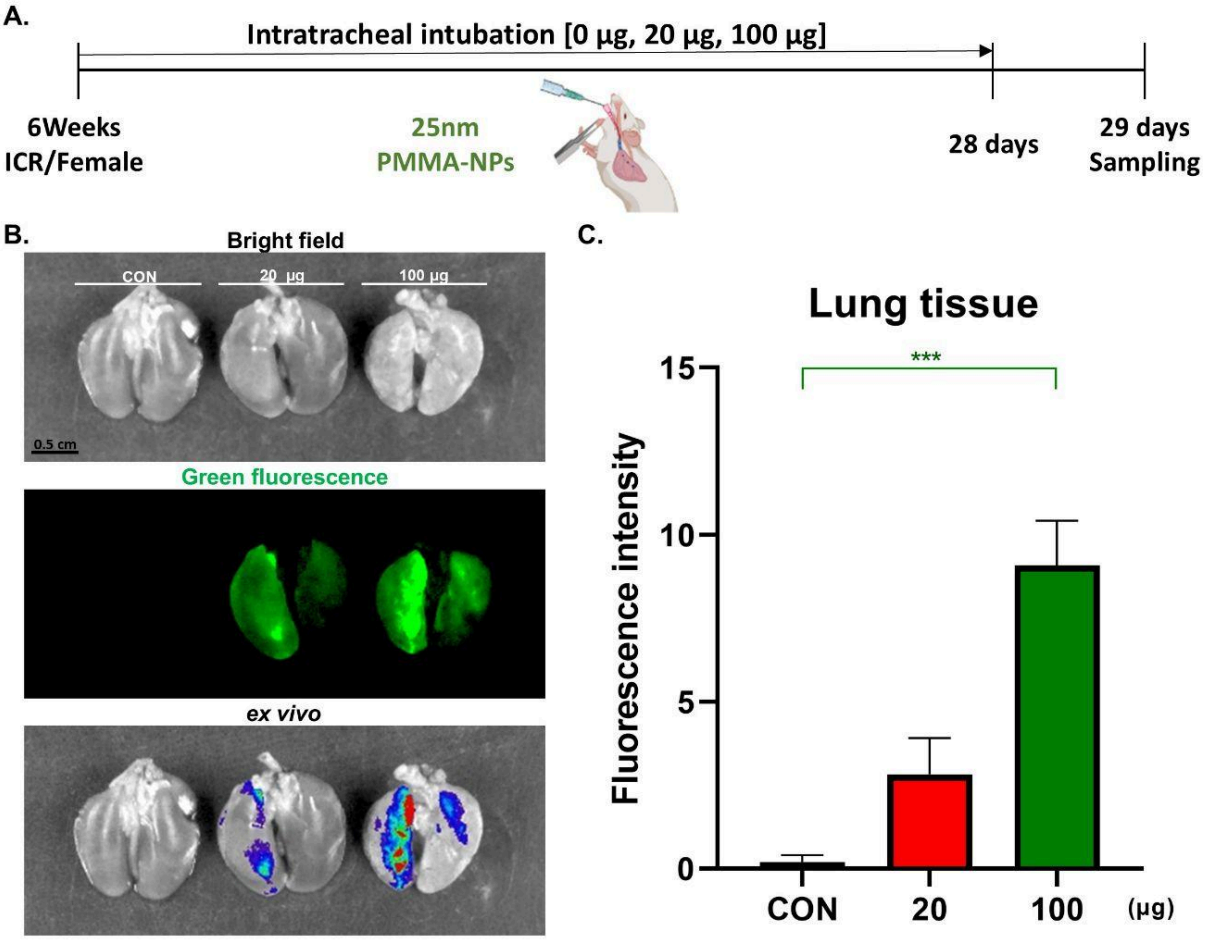

Fig. 1. Nanoplastics (NPs) inhaled through the airways accumulate in the lungs. (A) Schematic representation of the animal study design assessing the effects of NPs. (B, C) Green fluorescence of the whole lung tissue photographed with the *in vivo* imaging system. The fluorescence intensity was measured (n = 5, ordinary one-way ANOVA). Data are presented as the mean ± SEM. ***$p < 0.001$.

Result 2. Inhalation of NPs causes lung diseases.

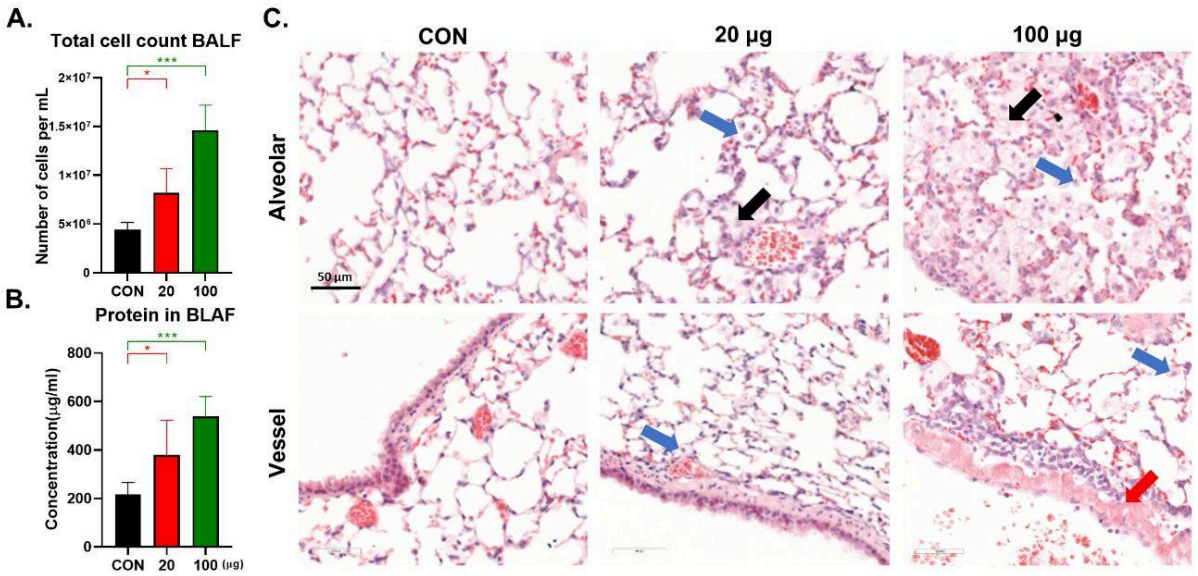

Fig. 2. Inhalation of NPs causes lung disease. (A, B) Cell counts and protein concentrations were quantified in bronchoalveolar lavage fluid (BALF; n = 5, ordinary one-way ANOVA). (C) Lung tissues were stained with hematoxylin and eosin (H&E). Blue arrows indicate macrophage, black arrows indicate foamy macrophages, and red arrows indicate lymphocytic infiltration. Data are presented as the mean ± SEM. *$p < 0.05$, ***$p < 0.001$.

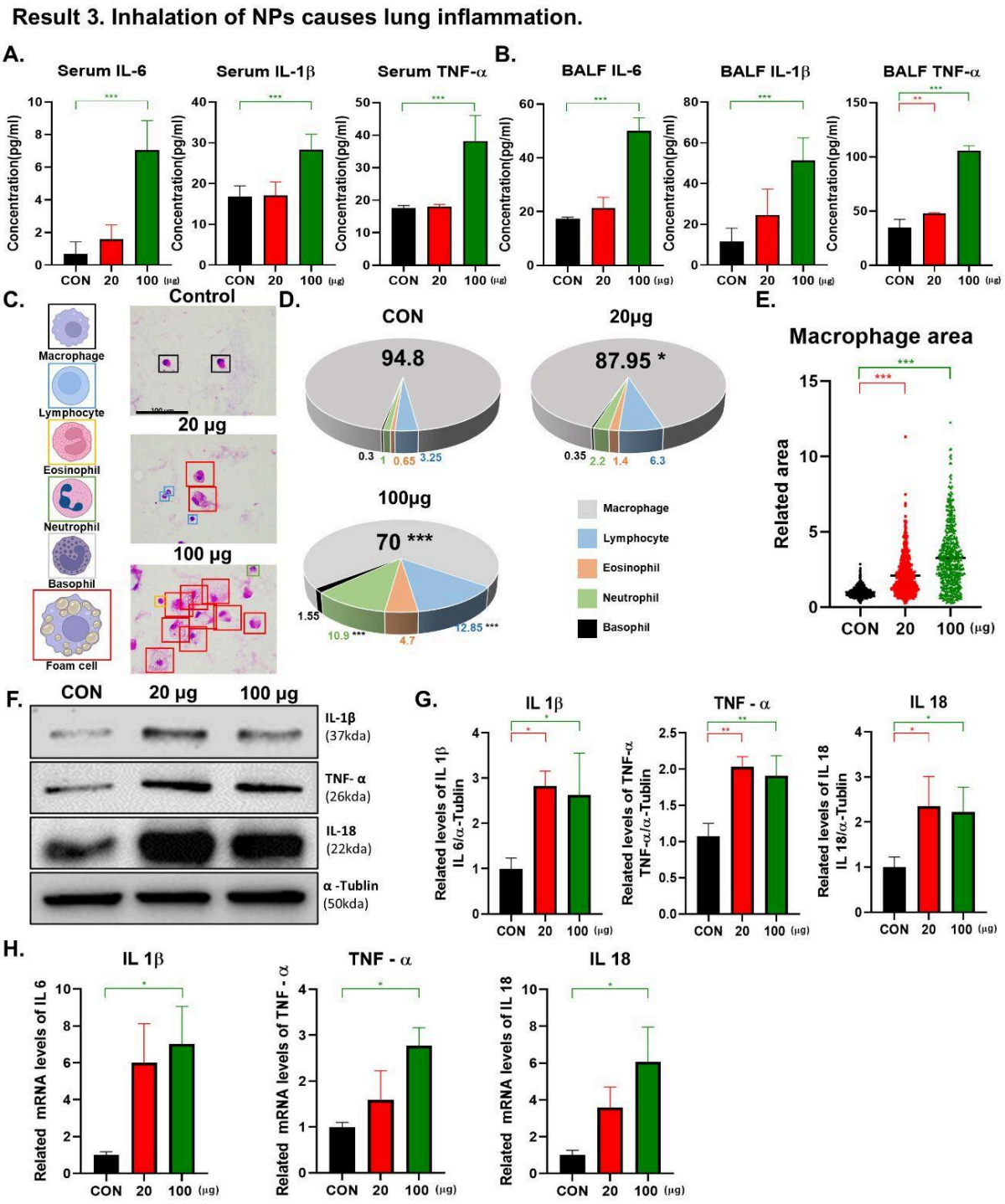

Fig. 3. NPs inhaled through the airways induce lung inflammation. (A, B) The levels of inflammatory cytokines in serum and bronchoalveolar lavage fluid (BALF) were measured using ELISA (n = 5, ordinary one-way ANOVA). (C, D) BALF cells were stained with hematoxylin and eosin staining (H&E) and 400 immune cells per mouse were classified (n = 5, ordinary one-way ANOVA). Black, red, blue, orange, and green squares represent alveolar macrophages, foamy macrophages, lymphocytes, represent eosinophils, and neutrophils, respectively. The area of 100 macrophages per mouse was measured (n = 5, ordinary one-way ANOVA). Inflammatory cytokine protein levels in lung tissue were determined by Western blotting (n = 3, ordinary one-way ANOVA). Inflammatory cytokine mRNA levels in lung tissue were determined by RT-qPCR (n = 4, ordinary one-way ANOVA). Data are presented as the mean ± SEM. **p < 0.01, ***p < 0.001.

Result 4. Inhalation of NPs causes profibrotic activation.

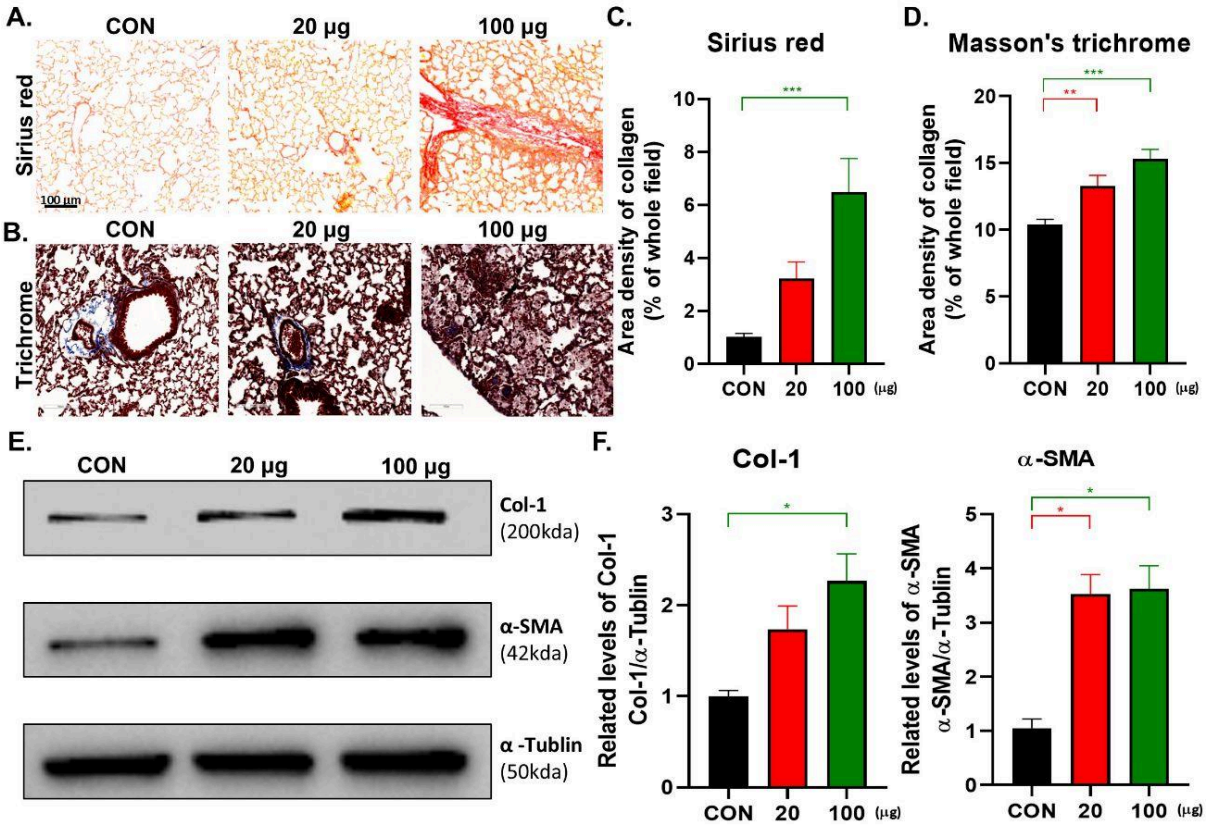

Fig. 4. NPs inhaled through the airways induce profibrotic activation. (A,B) Lung tissue slides were stained with Sirius red and Masson's trichrome to confirm fibrosis. (C,D) The percentage of fibrotic tissue is represented in a chart (n = 5, ordinary one-way ANOVA). (E) Fibrosis-related proteins were analyzed by Western blotting (n = 3, ordinary one-way ANOVA). Data are presented as the mean ± SEM. *p < 0.05, **p < 0.01, ***p < 0.001.